Exploring the Mechanism of *Blumea balsamifera* (L.) DC in Preventing and Treating Alzheimer's Disease Based on HPLC-ESI-HRMS and Network Pharmacology

Dong LI[1,2], Ling LI[2], Yujie HU[2], JiangXiong MA[1], Wenlong ZHANG[2], Chanyuan ZHOU[3], Dongsheng FAN[2], Xiaojian GONG[1]*

1. Key Laboratory for Information System of Mountainous Areas and Protection of Ecological Environment, Guizhou Normal University, Guiyang 550001, China; 2. Department of Pharmacy, the First Affiliated Hospital of Guizhou University of Traditional Chinese Medicine, Guiyang 550001, China; 3. College of Chemistry and Materials Engineering, Guiyang University, Guiyang 550005, China

Abstract [**Objectives**] To expose the plausible mechanism of *Blumea balsamifera* (L.) DC. against Alzheimer's disease via network pharmacology and HPLC-ESI-HRMS technology. [**Methods**] To begin with, HPLC-ESI-HRMS was employed to identify the components of *B. balsamifera*. Secondly, the potential targets of the components were identified and predicted based on chemical similarity and online databases. Thirdly, by way of topological analysis of a component-disease target interaction network, the primary candidate targets and potential active components were identified. Lastly, molecular docking analysis was used to confirm the interaction between active components and therapeutic targets. [**Results**] According to the final results, HPLC-ESI-HRMS identified 70 components. Out of these, 20 components were potentially biologically active, and most of them were sesquiterpenoids. According to the molecular docking results, the primary active components were appropriately coordinated with the core targets, indicating a high level of pharmacodynamic activity. Thus, the sesquiterpenes present in *B. balsamifera* are considered potential active ingredients having multi-target and multi-pathway effects for treating Alzheimer's disease. [**Conclusions**] This research will provide a scientific reference for the future pharmacological activity and clinical application of *B. balsamifera*.

Key words HPLC-ESI-HRMS, Alzheimer's disease, *Blumea balsamifera* (L.) DC., Network pharmacology, Molecular docking

1 Introduction

Alzheimer's disease (AD) is a prevalent neurodegenerative disorder, and it leads to irreversible neuron loss and cognitive impairment[1]. Its pathological features typically comprise of senile plaques that are extracellular aggregations of amyloid Aβ and neurofibrillary tangles that are intracellular aggregations of hyperphosphorylated Tau protein[2-3]. The prevalence of AD is rising due to rapid global aging, bringing significant economic and medical challenges to society. Research shows that 15.07 million individuals aged 60 years and over in China have dementia, with 9.83 million having AD. Additionally, there are around 6.5 million US citizens aged 65 years and over who suffer from AD. Without a breakthrough in the prevention, mitigation, or cure of AD, the number of patients is projected to increase to 13.8 million by 2060[1,4]. The cause of AD has not yet been fully comprehended. The AChE inhibitors Tacrine, Galanthamine and Memantine Hydrochloride, which have clinical applications and can alleviate patients' cognitive dysfunction, but they are unable to halt the progression of the disease. New drugs such as Sodium Oligomannate capsules and Aducanumab have recently received approval for use. Nevertheless, the clinical efficacy of these drugs needs to be further examined[5]. Therefore, it is imperative to identify drug candidates capable of reversing or terminating the pathological process of AD.

Blumea balsamifera (L.) DC (Asteraceae) is a plant with perennial herb or subshrub characteristics long employed for medicinal reasons in the ethnicminority regions of Miao, Zhuang, Li and others[6]. The essential oil of *B. balsamifera* contains (-)-borneol. Borneol is a significant active component present in *B. balsamifera*, which is frequently used in traditional Chinese medicine for its properties of 'resuscitation'. Borneol facilitates drug transportation across the blood-brain barrier and helps to enhance drug absorption in the brain[7-8]. Research indicates that (-)-borneol at a concentration of 100 μM protects SH-SY5 cells from Aβ-induced damage, reduces the production of reactive oxygen species, enhances the expression of HO-1 and nuclear translocation of Nrf2, has antioxidant properties, and increases the expression of Bcl-2 significantly. The inhibition of Aβ-induced apoptosis in SH-SY5Y cells was observed through a decrease in Bax expression[9]. The sesquiterpenoids and diterpenoids that have been extracted from *B. balsamifera* can substantially reduce the

Received: June 20, 2023 Accepted: September 6, 2023
Supported by Science and Technology Project of Guizhou Province of China (QKHPTRC [2021]259, QKH LH [2017] 7146); Doctoral Research Initiation Fund (GYZYYFY-BS-2018 [14]); 2018 Guizhou Provincial High Level Innovative Talent Project; Research Project on Traditional Chinese Medicine and Ethnic Medicine Science and Technology in Guizhou Province (QZYY2017-079, QZYY2017-087); Project of Key Laboratory Characteristic Forestry of Guizhou Province of China (QJHKY [2021] 002).
* Corresponding author. E-mail: gongxiaojian1@163.com

production of NO in microglia BV-2 cells and suppress neuroinflammation[10-11].

Based on the previous literature review[12], we analysed and identified the chemical components of *B. balsamifera* using HPLC-ESI-HRMS in this study. The active compounds from *B. balsamifera* with therapeutic properties for AD were screened by network pharmacology, and their mechanism of action was investigated and validated by molecular docking techniques. This research will offer a scientific reference for the future pharmacological activity and clinical application of *B. balsamifera*.

2 Material and methods

2.1 Materials

2.1.1 Materials and instruments. Acetonitrile (Xilong Chemical Co., Ltd), formic acid (Tianjin Hengxing Chemical Reagent Manufacturing Co., Ltd), methanol (Chongqing Wansheng Chuandong Chemical Co., Ltd), and water (self-made ultra-pure water) were used in the experiments. All other reagents were of analytical grade. *B. balsamifera* was collected from Ceheng County of Qianxinan Buyi and Miao Autonomous Prefecture, Guizhou Province. The medicinal material was identified as such by professor Zhang Wenlong at Guizhou University of Traditional Chinese Medicine.

Thermo Scientific Q exactive focus high resolution mass spectrometer, Dionex ultimate 3000 rslc liquid chromatograph, Electronic temperature control electric heating jacket 98-i-b (Tianjin Taist Instrument Co., Ltd.); Digital display thermostatic water bath hh-4 (Shanghai Lichen Bangxi Instrument Technology Co., Ltd.); Anheng electronic counter III ALM (Shenzhen Anheng Weighing Instrument Electronics Co., Ltd.); Pure water/ultrapure water system cleartm-d24uv (Merck Millipore); Ultrasonic cleaning machine kq-300de (Kunshan Ultrasonic Instrument Co., Ltd.); Electronic analytical balance xs10du [Mettler-Toledo Instrument (Shanghai) Co., Ltd.].

2.1.2 Preparation of test solution. The collected medicinal materials were dried naturally and then mixed by a grinder. About 1 g of medicinal material powder was weighed accurately, placed in a 100 mL round bottom flask, and added with 100 mL of methanol accurately. After extracted by reflux for 2 h, the solution was allowed to cool at rest, and filtered into a 100 mL measuring flask. The filtrate was made up to the scale with methanol and shaken well. Finally, the filtrate was filtered through a 0.2 μm microporous membrane.

2.2 Methods

2.2.1 Qualitative analysis by HPLC-ESI-HRMS. (i) Chromatographic conditions. Chromatographic column: Waters Acquity Uplc hss T3 (100 mm × 2.1 mm, 1.8 μm); Gradient elution mobile phase: 0.1% formic acid aqueous solution (B), acetonitrile (0.1% formic acid) (A); Specific elution conditions: 95% B (0-2 min), 95% -5% B(2-42 min), 5% B (42-47 min), 5% -95% B (47-47.1 min), 95% B (47.1-50 min). The flow rate was 0.3 mL/min and the column temperature was set at 40 ℃. The injection volume was 5 μL.

(ii) Mass spectrometric conditions. The following MS setup was used: Electrospray ionisation (ESI) source in positive and negative ion mode; Full scan high-resolution accurate-mass acquisition mode over the mass range of 100-1 500 *m/z*; Spectrum data type: Profile; Resolution: Full MS: 70 000, MS/MS: 17 500; Automatic gain control quantity: Full MS: 1×10^6, MS/MS: 2×10^5; Maximum IT: 100 ms (Full MS), 50 ms (MS/MS); Loop count: 3; MSX count: 1; Isolation width: 1.5 m/z; Step NCE: 20, 40, 60; Minimum AGC target: 8×10^3; Intensity threshold: 1.6×10^5; Spray voltage: positive ions 3.0 kV, negative ions 2.5 kV; Sheath gas flow rate: 35 psi; Auxgas flow rate: 10 psi; Sweep gas flow rate: 0; Capillary temperature: 320 ℃.

2.2.2 Data processing and component analysis. Based on the previous literature review, over 140 targets were collected and screened[12]. The HPLC-ESI-HRMS data underwent processing using Xcalibur 3.0. To allow comparison and analysis of the relative molecular weight, retention time (tR), fragment ion information, and fragmentation law of the target compound with the collected mass spectral data, Compound Discoverer 3.0 software was used. Abbreviations will be explained in the first instance of usage.

2.2.3 Screening of active ingredient from *B. balsamifera* and target collection. The chemical constituents of *B. balsamifera*, obtained by mass spectrometry and literature review, were screened for activity. Targets of the chemical constituents were obtained by entering the SMILES numbers of each constituent into the Swiss Target Prediction database, which predicts the targets of the constituents based on their 2D and 3D structures[13-14].

2.2.4 AD target collection. AD targets were obtained from three databases: Swiss Target Prediction[15] (http://swisstargetprediction.ch/), OMIM (https://www.omim.org/), and GeneCards (https://www.genecards.org/). The targets were then canonically calibrated to Gene ID (primary) by UniProt (https://www.uniprot.org/).

2.2.5 Construction of "active ingredient target" network. The active ingredients and intersection targets of *B. balsamifera* were imported into Cytoscape 3.8.2 software, and the "active ingredient target" network was constructed according to the corresponding attribute relationship.

2.2.6 Construction of protein-protein interaction network (PPI). The target information was obtained from STRING 11.5 (https://cn.string-db.org/) and imported into Cytoscape 3.8.2 software to construct the PPI network diagram.

2.2.7 Go function and KEGG enrichment analysis. Metasacpe database (https://metascape.org/gp/index.html#/main/step1) was used for GO and KEGG enrichment analysis of *B. balsamifera*-AD intersection targets. The collected data analysis results were visualized in the form of bubble maps.

2.2.8 Screening of key targets and active ingredients. The Analyze Network tool in Cytoscape 3.8.2 software was used for topological analysis, and the Cytohubba plug-in was used for degree cal-

culation. The top 5 target points in the PPI network were selected as key genes. Ten drugs highly correlated with *B. balsamifera* in the treatment of AD were selected as key drugs in the "*B. balsamifera* drug - target" network by MCC algorithm.

2.2.9 Molecular docking validation. The active ingredient's 2D structure was saved as a mol2 structure format. Then, the compound's 2D structure was converted to the 3D format and saved as a PDB format file using Open Babel 3.1.1 software. Subsequently, AutoDock Tools 4.2.6 was employed to convert the ligand molecule's 'pdbqt' format file. The crystal structure of the primary target was downloaded from the PDB database. Pre-processing of the receptor protein involved deleting water molecules, side chains, and ligands using PyMOL software. Subsequently, the receptor protein was transformed into the pdbqt format using Autodock Tools 4.2.6. Molecular docking was executed using AutoDock Vina 1.1.2, whereas the docking results were visualized by using PyMOL.

3 Results and analysis

3.1 Compound composition analysis Seventy compounds were identified by mass spectrometry, which were verified by comparison between the database (ChemSpider, MassBank, mzCloud) and references[16-29] (Table 1). Total ion chromatogram diagram of positive and negative ion modes of *B. balsamifera* sample is shown in Fig. 1.

Table 1 Identification of chemical constituents in *Blumea balsamifera* (L.) DC. by HPLC-ESI-HRMS

No.	Compound	Formula	Rt min	Detection value	Theoretical value	Error ppm	Ion type	Fragment ions (*m/z*)
1	Eriodictyol	$C_{15}H_{12}O_6$	17.16	287.056 2	287.055 0	1.225	$[M-H]^-$	151, 135
2	Eriodictyonone	$C_{16}H_{14}O_6$	21.30	301.071 8	301.070 7	1.115	$[M-H]^-$	135
3	Liquiritigenin	$C_{15}H_{12}O_4$	23.71	255.066 1	255.065 2	0.905	$[M-H]^-$	184, 171, 145, 125
4	5, 7, 3', 5'-Tetrahydroxydihydroflavanone	$C_{15}H_{12}O_6$	17.05	287.056 2	287.055 0	1.135	$[M-H]^-$	151, 135
5	Blumeatin	$C_{16}H_{14}O_6$	21.57	301.071 8	301.070 7	1.145	$[M-H]^-$	135, 143
6	(2S)-5, 7, 2', 5'-Tetrahydroxydihydroflavanone	$C_{15}H_{12}O_6$	16.82	287.056 2	287.055 0	1.165	$[M-H]^-$	151, 135
7	Isohemiphloin	$C_{21}H_{22}O_{11}$	15.02	449.108 9	449.107 8	1.082	$[M-H]^-$	339, 275, 244, 192, 177
8	(2R, 3R)-5-Methoxy-3, 5, 7, 2'-tetrahydroxydihydroflavone	$C_{15}H_{12}O_7$	12.84	303.051 1	303.049 9	1.131	$[M-H]^-$	253, 183, 145, 123
9	(2R, 3R)-7, 5'-Dimethoxy-3, 5, 2' -trihydroxydihydroflavone	$C_{17}H_{16}O_7$	20.61	333.097 0	333.096 9	0.071	$[M+H]^+$	296, 167, 137
10	(2R, 3R)-Dihydroquercetin-4'-methyl ether	$C_{16}H_{14}O_7$	15.91	317.066 7	317.065 6	3.566	$[M-H]^-$	277, 272, 256, 125, 105
11	(2R, 3R)-Dihydroquercetin-4', 7-dimethyl ether	$C_{17}H_{16}O_7$	20.76	333.096 9	333.096 9	0.041	$[M+H]^+$	225, 167, 137
12	7-O-methyltaxifolin	$C_{16}H_{14}O_7$	16.27	317.066 7	317.065 6	3.661	$[M-H]^-$	301
13	3, 3', 5, 5', 7-Pentahydroxydihydroflavone	$C_{15}H_{12}O_7$	13.69	303.051 1	303.049 9	1.131	$[M-H]^-$	296, 243, 212, 196, 138
14	Taxifolin	$C_{15}H_{12}O_7$	13.95	303.051 2	303.049 9	1.281	$[M-H]^-$	105, 92, 69
15	Cedeodarin	$C_{16}H_{14}O_7$	16.68	317.066 6	317.065 6	3.188	$[M-H]^-$	292, 237, 216
16	5, 7, 3', 4'-Tetrahydroxy-2-methoxy-3, 4-flavandione 3-hydrate	$C_{16}H_{14}O_9$	16.09	349.055 0	349.055 4	-1.199	$[M-H]^-$	274, 144, 131, 116
17	Luteolin	$C_{15}H_{10}O_6$	17.53	285.040 5	285.039 4	4.089	$[M-H]^-$	133
18	Luteolin 7-methyl ether	$C_{16}H_{12}O_6$	19.69	301.070 7	301.070 7	-0.048	$[M+H]^+$	215, 66
19	Velutin	$C_{17}H_{14}O_6$	22.04	313.071 9	313.070 7	4.042	$[M-H]^-$	243, 191, 109, 93
20	5, 4'-Dihydroxy-7-methoxyf lavone	$C_{16}H_{12}O_5$	23.82	283.061 2	283.060 1	3.957	$[M-H]^-$	189, 153, 117
21	Diosmetin	$C_{16}H_{12}O_6$	19.82	301.070 8	301.070 7	0.549	$[M+H]^+$	239, 209, 131, 88
22	Chrysoeriol	$C_{16}H_{12}O_6$	21.60	301.070 8	301.070 7	0.45	$[M+H]^+$	292, 192, 124
23	Quercetin	$C_{15}H_{10}O_7$	23.25	303.049 9	303.049 9	0	$[M+H]^+$	301, 273, 178
24	Ombuin	$C_{17}H_{14}O_7$	20.73	329.066 8	329.065 6	3.619	$[M-H]^-$	244, 153, 134, 128
25	Tamarixetin	$C_{16}H_{12}O_7$	20.20	315.051 2	315.049 9	4.066	$[M-H]^-$	150, 139, 128
26	Beta-rhamnocitrin	$C_{16}H_{12}O_7$	18.51	315.051 2	315.049 9	4.161	$[M-H]^-$	215, 104, 91, 68
27	3, 5, 7-Trihydroxy-3', 4'-dimethoxyflavone	$C_{17}H_{14}O_7$	20.75	329.066 8	329.065 6	3.71	$[M-H]^-$	259, 139, 119
28	Quercetin-3', 4', 7-trimethylether V	$C_{18}H_{16}O_7$	23.10	343.082 4	343.081 2	3.325	$[M-H]^-$	197, 175, 105, 85
29	5, 7'-Dimethoxy-3, 5, 2'-trihydroxyflavone	$C_{17}H_{14}O_7$	20.85	329.066 9	329.065 6	3.892	$[M-H]^-$	301, 208, 69, 55
30	Chrysosplenol C	$C_{18}H_{16}O_8$	8.97	359.077 1	359.076 1	0.916	$[M-H]^-$	335, 137, 116
31	Hyperoside	$C_{21}H_{20}O_{12}$	13.58	463.088 5	463.087 1	1.368	$[M-H]^-$	310, 195, 160
32	Quercetin 3'-methoxy-3-O-β-D-galactopyranoside	$C_{22}H_{22}O_{12}$	15.00	477.103 9	477.102 8	1.158	$[M-H]^-$	268, 218, 198
33	Isoquercitrin	$C_{21}H_{20}O_{12}$	13.35	463.088 4	463.087 1	1.278	$[M-H]^-$	237, 228, 147, 117
34	Ayanin	$C_{18}H_{16}O_7$	23.22	343.082 4	343.081 2	3.5	$[M-H]^-$	216, 169, 152, 121
35	Quercetin-3, 7, 3'-trimethyl ether	$C_{18}H_{16}O_7$	25.41	343.082 3	343.081 2	3.063	$[M-H]^-$	306, 232, 124, 105
36	Kumatakenin	$C_{17}H_{14}O_6$	25.00	313.071 8	313.070 7	3.659	$[M-H]^-$	166, 106, 93
37	Quercetin 3, 7-dimethyl ether	$C_{17}H_{14}O_7$	22.43	329.066 8	329.065 6	3.71	$[M-H]^-$	150, 130, 101, 90

(To be continued)

(Continued)

No.	Compound	Formula	Rt min	Detection value	Theoretical value	Error ppm	Ion type	Fragment ions (*m/z*)
38	Quercetin-3, 3', 4'-trimethyl ether	$C_{18}H_{16}O_7$	25.53	343.082 4	343.081 2	3.5	$[M-H]^-$	286, 262, 160
39	4', 5, 7-Trihydroxy-3, 3'-dimethoxyflavone	$C_{17}H_{14}O_7$	24.45	329.066 7	329.065 6	3.436	$[M-H]^-$	260, 226, 142
40	Quercetin-3, 4'-dimethyl ether	$C_{17}H_{14}O_7$	22.54	329.066 9	329.065 6	3.892	$[M-H]^-$	209, 206, 114
41	3', 4', 5, 7-Tetrahydroxy-3-methoxyflavone	$C_{16}H_{12}O_6$	21.71	301.070 7	301.070 7	0.25	$[M+H]^+$	251, 218, 103
42	Caulophyllogenin	$C_{15}H_{14}O_6$	18.26	289.071 9	289.070 7	4.274	$[M-H]^-$	177, 168, 134
43	Blumeaene A	$C_{20}H_{30}O_5$	19.69	351.214 1	351.216 6	−2.461	$[M+H]^+$	236, 195, 189, 109
44	Blumeaene B	$C_{20}H_{30}O_5$	19.75	351.214 1	351.216 6	−2.521	$[M+H]^+$	314, 257, 126
45	Blumeaene D	$C_{21}H_{32}O_5$	30.25	363.215 2	363.216 6	−1.361	$[M-H]^-$	285, 242, 175
46	Blumeaene E	$C_{20}H_{30}O_6$	17.60	365.197 9	365.195 9	2.015	$[M-H]^-$	218, 148, 118
47	Blumeaene F	$C_{20}H_{30}O_6$	18.42	365.196 8	365.195 9	0.915	$[M-H]^-$	173, 144
48	Blumpene B	$C_{20}H_{32}O_5$	27.31	353.231 7	353.232 3	−0.561	$[M+H]^+$	313, 266
49	Blumeaene E1	$C_{20}H_{30}O_6$	20.60	365.197 1	365.195 9	1.275	$[M-H]^-$	320, 279
50	Blumeaene E2	$C_{20}H_{30}O_6$	29.61	365.194 7	365.195 9	−1.165	$[M-H]^-$	315, 153, 64
51	Blumeaene M	$C_{20}H_{30}O_6$	27.48	365.197 2	365.195 9	1.335	$[M-H]^-$	155, 76
52	Balsamiferine E	$C_{20}H_{32}O_5$	27.33	353.231 8	353.232 3	−0.501	$[M+H]^+$	290, 121
53	Balsamiferine F	$C_{21}H_{32}O_5$	30.59	363.215 3	363.216 6	−1.271	$[M-H]^-$	236, 176, 155
54	Balsamiferine G	$C_{21}H_{32}O_5$	34.39	363.215 2	363.216 6	−1.361	$[M-H]^-$	171, 56
55	Blumpene D	$C_{21}H_{32}O_5$	30.55	363.215 2	363.216 6	−1.361	$[M-H]^-$	242, 111, 102
56	Blumeaene G	$C_{20}H_{30}O_5$	19.94	351.214 1	351.216 6	−2.461	$[M+H]^+$	356, 203
57	Blumeaene N	$C_{20}H_{30}O_6$	25.68	365.196 9	365.195 9	1.065	$[M-H]^-$	191, 126
58	Balsamiferine O	$C_{21}H_{34}O_7$	39.49	397.224 3	397.222 1	2.22	$[M-H]^-$	315, 159, 145
59	Blumeaene I	$C_{20}H_{30}O_6$	22.97	365.196 9	365.195 9	1.005	$[M-H]^-$	248, 243, 111
60	Balsamiferine I	$C_{20}H_{30}O_5$	21.24	351.213 8	351.216 6	−2.821	$[M+H]^+$	164, 149, 57
61	Balsamiferine J	$C_{20}H_{30}O_5$	21.26	351.213 7	351.216 6	−2.891	$[M+H]^+$	164, 154, 78
62	Inuchinenolide B	$C_{17}H_{22}O_5$	10.97	305.141 1	305.138 4	2.79	$[M-H]^-$	124, 80
63	Neogaillardin	$C_{17}H_{22}O_5$	11.00	305.141 5	305.138 4	3.1	$[M-H]^-$	164
64	Blumealactone A	$C_{20}H_{28}O_6$	26.37	363.181 0	363.180 2	0.785	$[M-H]^-$	363
65	Balsamiferine D	$C_{20}H_{34}O_4$	26.03	337.238 5	337.237 3	1.154	$[M-H]^-$	212, 152, 69
66	Balsamiferine C	$C_{15}H_{24}O_3$	10.16	253.179 7	253.179 8	−0.151	$[M+H]^+$	104
67	(4*R*, 5*R*)-4, 5-Dihydroxycaryophyll-8(13)-ene	$C_{15}H_{24}O$	26.97	221.189 9	221.190 0	−0.142	$[M+H]^+$	139
68	Balsamiferine R	$C_{20}H_{30}O_6$	23.04	365.196 8	365.195 9	0.975	$[M-H]^-$	192, 173
69	(7*S*, 12*Z*)-12, 14-Labdadiene-7, 8-diol	$C_{20}H_{34}O_2$	24.88	307.226 4	307.226 4	−0.361	$[M+H]^+$	307
70	Austroinulin	$C_{20}H_{34}O_3$	37.95	323.257 1	323.258 1	−1.021	$[M+H]^+$	323, 211

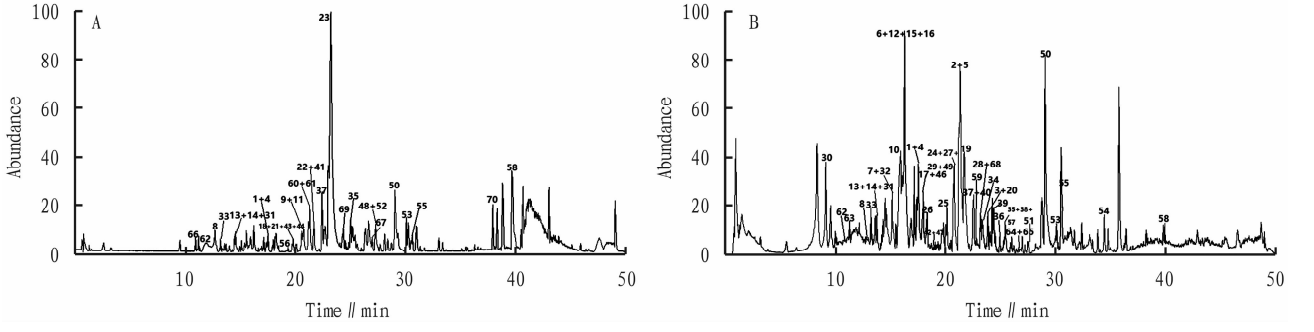

Fig. 1 Total ion chromatograms (TIC) of *Blumea balsamifera* (L.) DC in positive (A) and negative (B) modes

3.2 Screening of active ingredients of *B. balsamifera* Twenty active compounds were screened using the SwissADME online database under reference conditions of gastrointestinal absorption, druglikeness, and blood-brain barrier permeability (Table 2). These compounds, which include one flavonoid, 17 sesquiterpenoids, and 2 diterpenes, are presented in Fig. 2.

3.3 Collection of active ingredients and AD targets of *B. balsamifera* The possible targets of the active ingredients were acquired, resulting in 239 targets. A total of 1 966 targets were related to AD. The Venny 2.1.0 Online Tool was used to

find the intersection of the active ingredient targets and AD targets, leading to a total of 93 intersected targets (Fig. 3).

Table 2 Active ingredients

No.	Compound	No.	Compound
19	Velutin	60	Balsamiferine I
44	Blumeaene B	61	Balsamiferine J
45	Blumeaene D	62	Inuchinenolide B
46	Blumeaene E	63	Neogaillardin
52	Balsamiferine E	64	Blumealactone A
53	Balsamiferine F	65	Balsamiferine D
54	Balsamiferine G	66	Balsamiferine C
57	Blumeaene N	68	Balsamiferine R
58	Balsamiferine O	69	(7*S*,12*Z*)-12,14-Labdadiene-7,8-diol
59	Blumeaene I	70	Austroinulin

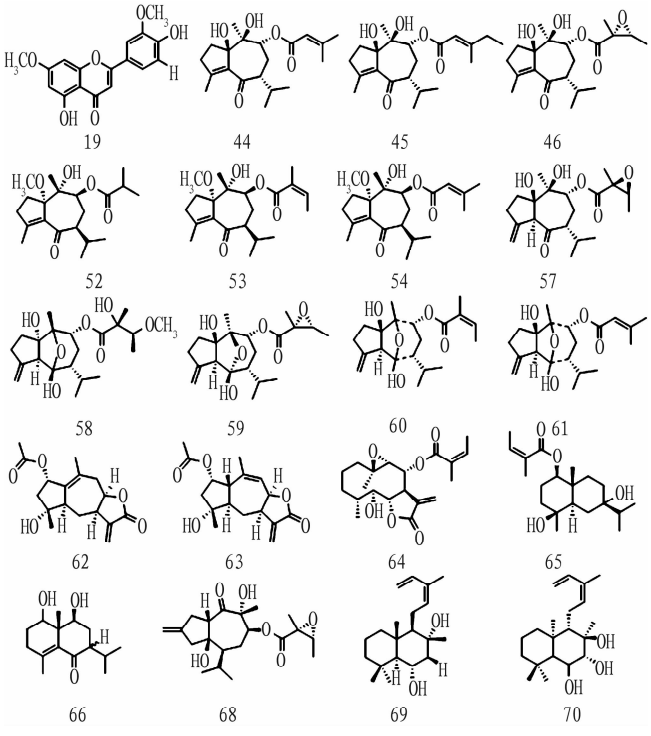

Fig. 2 Structure of active ingredients

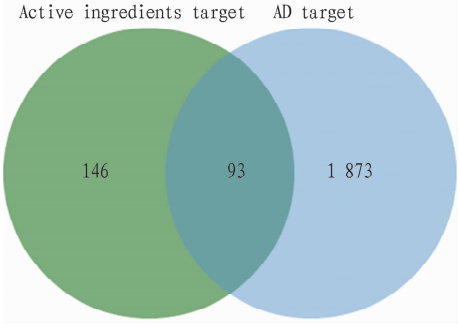

Fig. 3 Venn diagram of active ingredients target and AD target

3.4 Construction of "active ingredient-target" network and screening of main active ingredients To create an "active ingredient intersection target" network diagram, which includes 268 interacting nodes and 555 edges (Fig. 4), the active ingredients and intersection targets of *B. balsamifera* were imported into the Cytoscape 3.8.2 software. The network underwent topology analysis using the Analyze Network tool. By using the Cytohubba plug-in for MCC algorithm, 10 primary active ingredients, including 8 sesquiterpenes and 2 diterpenoids, were identified.

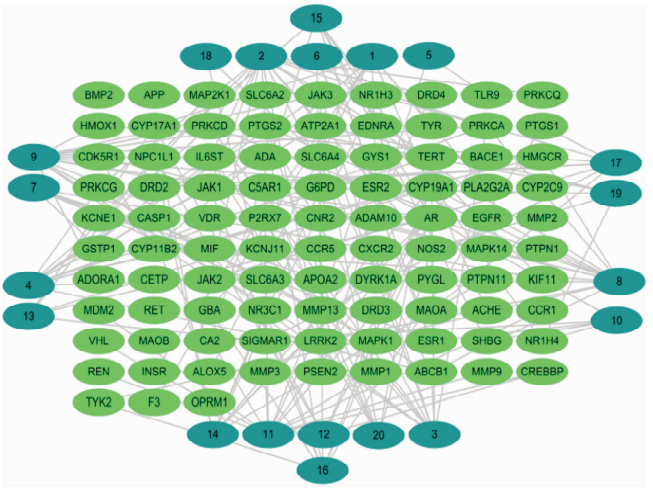

Fig. 4 Network diagram of "active ingredient-target"

3.5 Construction of PPI and screening of key targets Ninety-three intersection targets that had been screened were entered into the String 11.5 database to create the network diagram. Then, the TSV file exported was imported into Cytoscape 3.8.2 software to build the PPI network diagram (Fig. 5). Out of these, Cytohubba plug-in calculated and screened 5 significant gene targets with the following degrees: EGFR (degree = 86), PTGS2 (degree = 74), ESR1 (degree = 68), MMP9 (degree = 62), and MAPK1 (degree = 58). All of these values significantly exceeded the median degree of 20. These significant gene targets exhibited strong interactions not only with other targets but also with 20 active ingredients, thus highlighting their importance and potential clinical significance.

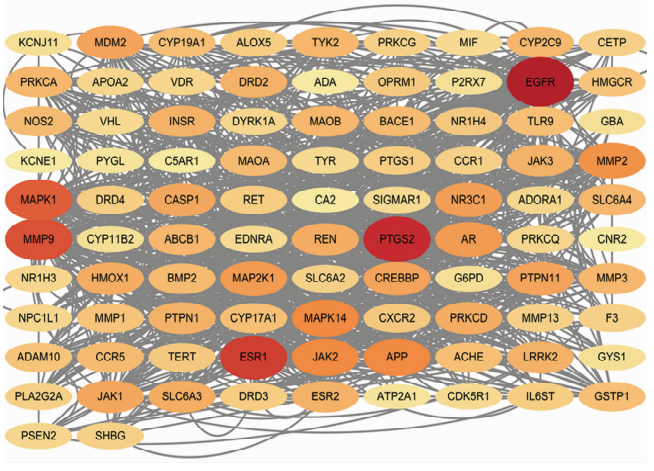

Fig. 5 PPI network diagram

3.6 Go function and KEGG enrichment analysis The Metascape database was used to perform GO enrichment analysis

($P<0.05$), resulting in a total of 466 entries for biological processes. The top 10 analysis results with P values were displayed (Fig. 6). Of these, 244 biological processes were enriched (accounting for 52.36% of the total items), mainly related to the response of cells to nitrogen compounds, hormones, inflammation, inorganic substances, as well as the regulation of MAPK cascade, defense response, system process, and other biological processes. A total of 126 molecular functions were enriched, representing 27.04% of the total items. These functions were mainly related to the activity of protein serine/threonine/tyrosine kinase, non-membrane spanning protein tyrosine kinase, endopeptidase, and MAP kinase, as well as the regulation of steroid binding and phosphatase binding. A total of 96 cellular components were enriched, accounting for 20.60% of the total items. Most targets were distributed in membrane rafts, neuronal cell bodies, perinuclear cytoplasm, membrane side, neuromuscular junctions, and other regions. This shows that the active components of *B. balsamifera* treat AD through multiple GO functions.

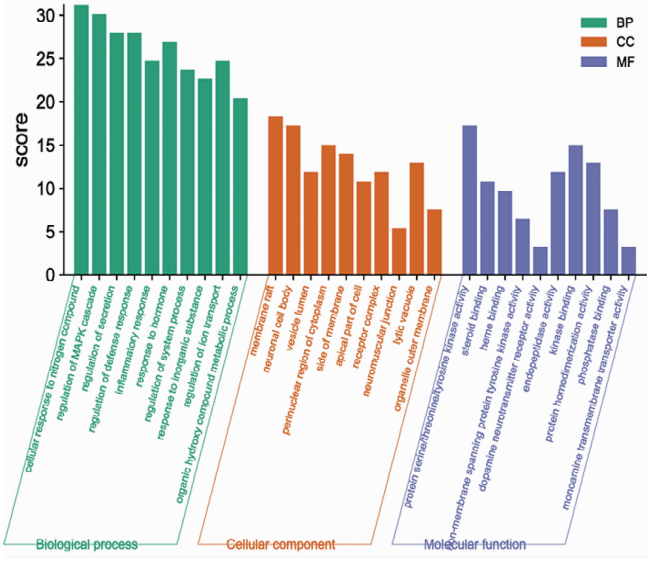

Fig. 6 GO function enrichment analysis

The KEGG pathway enrichment analysis ($P<0.05$) revealed that 158 pathways were enriched. The top 20 analysis results with P values were chosen for display in the bubble diagram (Fig. 7). The involved pathways consist of the cancer pathway, 5-serotonergic synaptic pathway, HIF-1 signalling pathway, hepatitis B pathway, chemokine signalling pathway, cMAP signalling pathway, dopaminergic synaptic pathway, *etc*. Multiple diseases involving neurodegenerative pathways and receptor interactions of neuroactive ligands suggest that the active ingredient of *B. balsamifera* is a treatment involving multiple pathways for AD.

3.7 Molecular docking verification results The 10 primary active ingredients (Table 3) chosen based on Section **3.4** were subjected to docking with their respective key targets (Table 4). The prominent active ingredient was defined as a small molecule ligand, and the key target was identified as a receptor protein. Docking verification was done using AutoDock Vina 1.1.2. The docking results are shown in Table 5.

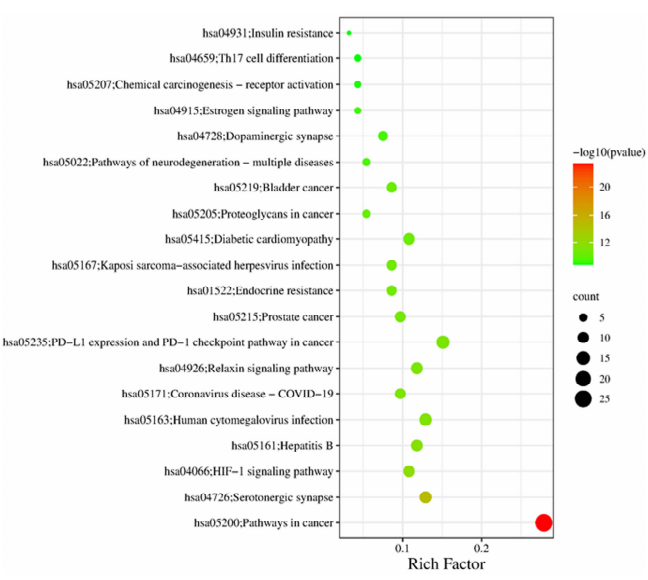

Fig. 7 KEGG pathway enrichment analysis

Table 3 Main active ingredients

No.	Compound	Corresponding key targets
1	Balsamiferine E	PTGS2
2	Balsamiferine F	PTGS2
3	Balsamiferine G	PTGS2
4	Balsamiferine I	ESR1
5	Balsamiferine J	ESR1
6	Inuchinenolide B	PTGS2
7	Neogaillardin	PTGS2, MAPK1
8	Balsamiferine D	MMP9
9	(7*S*,12*Z*)-12,14-Labdadiene-7,8-diol	ESR1
10	Austroinulin	ESR1

Table 4 Key target information

No.	Gene name	Name	Degree	PDB ID	Ligand small molecule
A	EGFR	Epidermal growth factor receptor	86	2J5F	DJK
B	MAPK1	Mitogen-activated protein kinase 1	58	1PME	SB2/SO4
C	ESR1	Estrogen receptor	68	1A52	EST/AU
D	PTGS2	Prostaglandin G/H synthase 2	74	1CVU	ACD/BOG/NAG
E	MMP9	Matrix metalloproteinase-9	62	1GKC	NFH/ZN/CA

The results showed that the binding energies of the main active ingredients to the key targets ranged from −6.3 to −8.8 kcal/mol. In order to compare the accuracy of structure prediction, we used the distance metric RMSD between the experimental and predicted structures. The RMSD value is based on the symmetry, partial symmetry and approximate symmetry in a simple heuristic way. In short, the RMSD value is the structural difference between two molecules (or between two states of the same molecule). The smaller the value, the greater the docking reliability. When it is less than 2 Å, the docking accuracy is higher[32-35]. In order to determine the binding activity and binding sites of components and target proteins, six docking results with the lowest docking energy were selected, and the RMSD values and hydrogen bonds within the docking range of the six results were calculated by PyMOL software (Table 6) and visualized (Fig. 8).

Table 5 Docking results

No.	Binding energy//kcal/mol			
	B	C	D	E
1	–	–	-6.3	–
2	–	–	-7.0	–
3	–	–	-7.3	–
4	–	-8.5	–	–
5	–	-8.8	–	–
6	–	–	-8.1	–
7	-8.3	–	-8.0	–
8	–	–	–	-7.5
9	–	-8.8	–	–
10	–	-8.1	–	–

Note: The smaller the binding energy is, the more stable the binding conformation is; the binding energy less than -5.0 kcal/mol indicates that the binding activity between them is better, and that less than -8.0 kcal/mol indicates a strong binding activity[30-31].

Table 6 RMSD and hydrogen bond

Result	No.	RMSD//Å	Hydrogen bond//3 Å
5-C	A	2.388	HIS-524, LEU-384, ARG-394
6-C	B	2.306	THR-347, LEU-428
7-D	C	2.981	THR-2206, ASN-2382, THR-2212, HIS-2214, ARG-2222
8-B	D	2.637	LYS-114
9-C	E	3.044	ARG-394, LEU-428, ILE-424
10-C	F	2.239	LEU-384, MET-388, ARG-394

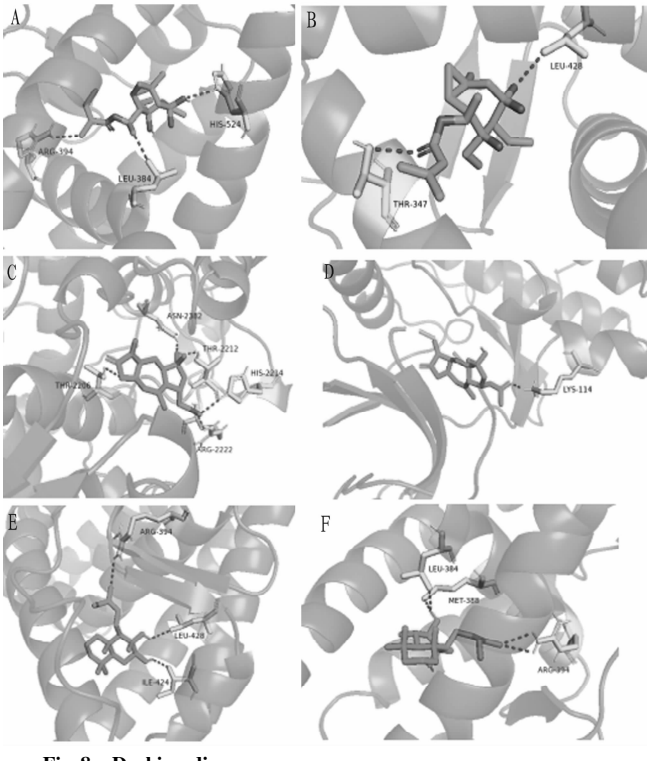

Fig. 8 Docking diagram

4 Discussion

Recently, the rapid advancement of computer simulation technologies, including network pharmacology, molecular docking, and pharmacophore modelling, has introduced novel approaches to unveil the material foundation and operation mechanism of traditional Chinese medicine and compounding. It has also brought new techniques for compound activity screening whilst considerably reducing the time and cost associated with discovering active compounds[36]. This study screened 29 active components, mostly terpenoids and mainly sesquiterpenes, from *B. balsamifera* using HPLC-ESI-HRMS combined with network pharmacology. Previous studies have reported that sesquiterpenes, which were isolated from *B. balsamifera*, can significantly inhibit the production of NO by BV-2 microglial cells induced by lipopolysaccharide. This inhibition can lead to the suppression of neuroinflammation[10-11]. The above findings suggest that sesquiterpenes may be the primary active component with anti-AD properties in *B. balsamifera*.

AD is a degenerative neurological condition with a complex origin. In recent decades, while significant progress has been made in the molecular and cellular studies concerning AD pathology, scientists are still endeavouring to develop innovative strategies for the treatment of the condition[37].

Research has shown the importance of estrogen in maintaining normal brain function. Moreover, estrogen receptors α and β (ESR1 and ESR2) have a strong correlation with the development of AD, and estrogen slows down the progression of AD[38]. ESR1 might protect memory from impairment by stimulating Aβ degradation and down-regulating amyloidosis as well as neurogenic inflammation in knockout ESR1 mouse model experiments[39]. The levels of ERRα and mRNA regions reduce with age in the APP/PS1 mouse model. Overexpression of ERR1 in HEK293 cells inhibits amyloidosis process in APP, reducing Aβ1-40/1-42 levels. Moreover, ERR1 overexpression in HEK/APP cells reverses APP and Tau phosphorylation alterations caused by hydrogen peroxide[40-41]. Therefore, ERR1 shows potential as a therapeutic target for AD.

The MAPK pathway plays a crucial role in transmitting signals from the outer membrane of a cell to the interior of the nucleus, ultimately regulating numerous cellular activities like proliferation, differentiation, apoptosis, survival, inflammation, and innate immunity[42]. In the adult brain, ERK is abundant and plays a significant role in regulating neuronal function. Additionally, the ERK pathway can serve multiple roles in activity-dependent regulation of neuronal function[43]. In a mouse model of LPS-induced memory damage, trans-cinnamaldehyde accelerates the destabilization of the mRNA for inducible nitric oxide synthase (iNOS) by disrupting the mitogen-activated protein kinase ERK1/2 pathway. This observation significantly reduces the production of nitric oxide (NO) in microglia and decreases inflammatory damage[44]. Additionally, the modulation of the RAS/MEK/ERK signalling pathway, by modulating the expression of MEK, p-MEK, ERK, and p-ERK, considerably improves cognitive performance and reduced

pathological damage in AD mice[45].

*PTGS*2 is the gene that encodes for cyclooxygenase-2 (COX-2), an enzyme responsible for the conversion of arachidonic acid to prostaglandins (PG). It plays a crucial role in several inflammatory processes as well as normal functions in neurons. In the hippocampal and cortical neurons, COX-2 expression regulates neuroplasticity through PG production[46]. Research has indicated that pharmacological inhibition of COX-1/2 can aim at pathophysiological mechanisms that oppose AD's progression by regulating processes upstream and downstream of Aβ and Tau[47]. Dysregulation of COX-2 causes abnormal cleavage of the β-amyloid precursor protein, and leads to the aggregation and deposition of Aβ as well as phosphorylated Tau tangles[48-50].

In the central nervous system, MMPs can be produced by all brain cells and are associated with neurogenesis, neuronal plasticity, and other physiological activities of the nervous system. Studies have shown that increased levels of MMP expression in AD may contribute to or interfere with the pathophysiological mechanisms of the disease[51]. Of these, MMP-9 is expressed in responsive astrocytes that encircle amyloid plaques. Its capability to break down soluble Aβ and amyloid plaques into non-toxic fragments supports neuron protection[52]. The cognitive impairment caused by Aβ *in vivo* and neurotoxicity *in vitro* can be significantly alleviated in MMP-9 pure knockout (KO) mice and by administering MMP inhibitors[53]. Moreover, inhibiting MMP9 can improve certain neurobehavioral deficits associated with AD, like anxiety and social recognition memory[53].

Molecular docking techniques were utilized to investigate the binding ability of the 10 primary active ingredients to their key targets. According to the results, the main active ingredients created a robust affinity with the ao acid residues of the key targets by hydrogen bonding, indicating a high level of potent activity. Nonetheless, the molecular docking technique possesses a few limitations because it does not reflect directly whether the binding action of the component to the target is inhibitory or activating[54].

In conclusion, this research has made preliminary conclusions regarding the active components and mode of action of *B. balsamifera* in the treatment of AD through HPLC-ESI-HRMS and network pharmacology. This provides a theoretical foundation for studying the pharmacological mechanisms of *B. balsamifera*. Nevertheless, the findings of this study are derived from the network pharmacology approach and are presently limited to theoretical analyses. To achieve a complete comprehension of its mechanism of action and to advance the research and development of *B. balsamifera* as an ethnomedicine, further substantiation via both *in vitro* and *in vivo* investigations is necessary. This could further provide valuable insights and scientific references.

References

[1] 2022 Alzheimer's disease facts and figures[J]. Alzheimer's & Dementia: The Journal of the Alzheimer's Association, 2022,18(4): 700-789.

[2] HOLTZMAN DM, MORRIS JC, GOATE AM. Alzheimer's disease: The challenge of the second century[J]. Science Translational Medicine, 2011, 3(77): 77sr1.

[3] FOLEY P. Lipids in Alzheimer's disease: A century-old story[J]. Biochimica et Biophysica Acta, 2010, 1801(8): 750-753.

[4] REN R, QI J, LIN S, *et al*. The China Alzheimer Report 2022[J]. General Psychiatry, 2022, 35(1): e100751.

[5] ZHANG P, JI H, HU QH. Research progress in clinical treatment of Alzheimer's disease and potential drugs from natural products[J]. Acta Pharmaceutica Sinica, 2022,57(7):1954-1961. (in Chinese).

[6] Editorial board of flora of China, Chinese Academy of Sciences. Flora of China[M]. Beijing: Science Press, 1979. (in Chinese).

[7] ZHANG QL, FU BM, ZHANG ZJ. Borneol, a novel agent that improves central nervous system drug delivery by enhancing blood-brain barrier permeability[J]. Drug Delivery, 2017, 24(1): 1037-1044. (in Chinese).

[8] LIANG XC, CHEN ZR, XU JK, *et al*. Effects of L-borneol on chloride channel and cell volume in human umbilical vein endothelial cells[J]. Chinese Pharmacological Bulletin, 2018, 34(4): 550-556. (in Chinese).

[9] HUR J, PAK SC, KOO BS, *et al*. Borneol alleviates oxidative stress via upregulation of Nrf2 and Bcl-2 in SH-SY5Y cells[J]. Pharmaceutical Biology, 2013, 51(1): 30-35.

[10] XU J, JIN DQ, LIU C, *et al*. Isolation, characterization, and NO inhibitory activities of sesquiterpenes from *Blumea balsamifera*[J]. Journal of Agricultural and Food Chemistry, 2012, 60(32): 8051-8058.

[11] MA J, REN Q, DONG B, *et al*. NO inhibitory constituents as potential anti-neuroinflammatory agents for AD from *Blumea balsamifera*[J]. Bioorganic Chemistry, 2018(76): 449-457.

[12] FAN DS, LI L, WANG KK, *et al*. Research progress on chemical constituents and pharmacological activities of *Blumea balsamifera*[J]. China Pharmacy, 2022, 33(10): 1274-1280. (in Chinese).

[13] DAINA A, MICHIELIN O, ZOETE V. SwissADME: A free web tool to evaluate pharmacokinetics, drug-likeness and medicinal chemistry friendliness of small molecules[J]. Scientific Reports, 2017(7): 42717.

[14] DAINA, ANTOINE, ZOETE, *et al*. A BOILED-Egg to predict gastrointestinal absorption and brain penetration of small molecules[J]. ChemMedChem, 2016, 11(11): 1117-1121.

[15] DAINA A, MICHIELIN O, ZOETE V. SwissTargetPrediction: Updated data and new features for efficient prediction of protein targets of small molecules[J]. Nucleic Acids Research, 2019, 47(W1): W357-W364.

[16] KOKANOVA-NEDIALKOVA Z, NEDIALKOV PT. UHPLC-HRMS based flavonoid profiling of the aerial parts of *Chenopodium foliosum* Asch. (Amaranthaceae)[J]. Natural Product Research, 2021, 35(19): 3336-3340.

[17] TSUGAWA H, NAKABAYASHI R, MORI T, *et al*. A cheminformatics approach to characterize metabolomes in stable-isotope-labeled organisms[J]. Nature Methods, 2019, 16(4): 295-298.

[18] AN HM, HUANG DR, YANG H, *et al*. Comprehensive chemical profiling of Jia-Wei-Qi-Fu-Yin and its network pharmacology-based analysis on Alzheimer's disease[J]. Journal of Pharmaceutical and Biomedical Analysis, 2020(189):113467.

[19] CHEN M, QIN JJ, FU JJ, *et al*. Blumeaenes A-J, sesquiterpenoid esters from *Blumea balsamifera* with NO inhibitory activity[J]. Planta Medica, 2010, 76(9): 897-902.

[20] LI Y, LIU J, WU Y, *et al*. Guaiane-type sesquiterpenes from Curcuma-

wenyujin[J]. Phytochemistry, 2022(198): 113164.
[21] SHIROTA O, ORIBELLO JM, SEKITA S, *et al.* Sesquiterpenes from *Blumea balsamifera*[J]. Journal of Natural Products, 2011, 74(3): 470 – 476.
[22] TIAN SH, ZHANG C, ZENG KW, *et al.* Sesquiterpenoids from *Artemisia vestita*[J]. Phytochemistry, 2018(147): 194 – 202.
[23] WANG Y, HARRINGTON PB, CHEN P. Analysis of phenolic compositions in cranberry dietary supplements using UHPLC-HRMS[J]. Journal of Food Composition and Analysis, 2020(86): 103362.
[24] ZHOU W, WANG PG. Simultaneous determination of multi-class active pharmaceutical ingredients by UHPLC-HRMS[J]. Journal of Pharmaceutical and Biomedical Analysis, 2021(202): 114160.
[25] CHEN Y, GAO CX, YE CS, *et al.* Qualitative analysis and identification of chemical constituents of Wumei pills based on UHPLC-Q-Orbitrap HRMS[J]. Journal of Chinese Medicinal Materials, 2022, 45(9): 2151 – 2156. (in Chinese).
[26] LIU CH, XIE JL, FU CL, *et al.* Qualitative and quantitative study of constituents in Lysionoti Herba using UHPLC-Q-Exactive Orbitrap HRMS and HPLC-UV[J]. China Journal of Chinese Materia Medica, 2023, 48(13): 3516 – 3534. (in Chinese).
[27] WANG YL, HUANG JG, LIU CJ, *et al.* Chemical profiling and tissue distribution study of Huanglian Jiedu Decoction in rats by UHPLC-O-Exactive Orbitrap HRMS[J]. Chinese Traditional and Herbal Drugs, 2022, 53(22): 6985 – 7000. (in Chinese).
[28] WANG Y, YU GF, HU JH, *et al.* Exploring the effective components and mechanism of Maxing Zhixiao granules in the treatment of asthma based on UPLC-Q-TOF-MS/MS and network pharmacology[J]. Chinese Traditional and Herbal Drugs, 2023, 54(17): 5508 – 5521. (in Chinese).
[29] YANG H, ZENG L, ZHENG ZX, *et al.* Analysis of chemical constituents of *Prinsepia utilis* Royle based on UHPLC-Q/Orbitrap HRMS[J]. Journal of Chinese Medicinal Materials, 2022,45(9): 2144 – 2150. (in Chinese).
[30] TROTT O, OLSON AJ. AutoDock Vina: Improving the speed and accuracy of docking with a new scoring function, efficient optimization, and multithreading[J]. Journal of Computational Chemistry, 2010, 31(2): 455 – 461.
[31] CAI JL, LI XP, ZHU YL, *et al.* Mechanism of Huangjing Qianshi Decoction in treatment of prediabetes based on network pharmacology and molecular docking[J]. China Journal of Chinese Materia Medica, 2022, 47(4): 1039 – 1050. (in Chinese).
[32] BELL EW, ZHANG Y. DockRMSD: An open-source tool for atom mapping and RMSD calculation of symmetric molecules through graph isomorphism[J]. Journal of Cheminformatics, 2019, 11(1): 40.
[33] KADUKOVA M, GRUDININ S. Docking of small molecules to farnesoid X receptors using AutoDock Vina with the Convex-PL potential: Lessons learned from D3R Grand Challenge 2[J]. Journal of Computer-Aided Molecular Design, 2017, 32(1): 151 – 162.
[34] KOEBEL MR, SCHMADEKE G, POSNER RG, *et al.* AutoDock VinaXB: Implementation of XBSF, new empirical halogen bond scoring function, into AutoDock Vina[J]. Journal of Cheminformatics, 2016 (8): 27.
[35] LIU C, LIU L, LI J, *et al.* Virtual screening of active compounds from jasminum lanceolarium and potential targets against primary dysmenorrhea based on network pharmacology[J]. Natural Product Research, 2021, 35(24): 5853 – 5856.
[36] XU MX, CHEN SK, GUAN TB, *et al.* Discovery of active ingredients against *Pseudomonas aerucinosa* from traditional Chinese medicine based on Virtua screening[J]. Chemical Research and Application, 2022, 34 (4): 754 – 763. (in Chinese).
[37] MATHEW A, BALAJI EV, PAI SRK, *et al.* Current drug targets in Alzheimer's associated memory impairment: A comprehensive review [J]. CNS Neurol Disord Drug Targets, 2023, 22(2): 255 – 275.
[38] JANICKI SC, SCHUPF N. Hormonal influences on cognition and risk for Alzheimer's disease[J]. Current Neurology and Neuroscience Reports, 2010, 10(5): 359 – 366.
[39] HWANG CJ, YUN HM, PARK KR, *et al.* Memory impairment in estrogen receptor alpha knockout mice through accumulation of amyloid-beta peptides[J]. Molecular Neurobiology, 2015, 52(1): 176 – 186.
[40] TANG Y, MIN Z, XIANG XJ, *et al.* Estrogen-related receptor alpha is involved in Alzheimer's disease-like pathology[J]. Experimental Neurology, 2018(305): 89 – 96.
[41] MURAKAMI K, SHIMIZU T, IRIE K. Formation of the 42-mer amyloid beta radical and the therapeutic role of superoxide dismutase in Alzheimer's disease [J]. Journal of Amino Acids, 2011 (2011): 654207.
[42] KIM EK, CHOI EJ. Compromised MAPK signaling in human diseases: an update[J]. Archives of Toxicology, 2015, 89(6): 867 – 882.
[43] ZHU X, LEE H G, RAINA AK, *et al.* The role of mitogen-activated protein kinase pathways in Alzheimer's disease [J]. Neuro-signals, 2002, 11(5): 270 – 281.
[44] ZHANG P, XU S, ZHU Z, *et al.* Multi-target design strategies for the improved treatment of Alzheimer's disease[J]. European Journal of Medicinal Chemistry, 2019(176): 228 – 247.
[45] LI H, LEI T, ZHANG J, *et al.* Longan (*Dimocarpus longan* Lour.) aril ameliorates cognitive impairment in AD mice induced by combination of D-gal/AlCl3 and an irregular diet via RAS/MEK/ERK signaling pathway[J]. Journal of Ethnopharmacology, 2021(267): 113612.
[46] YANG H, CHEN C. Cyclooxygenase-2 in synaptic signaling[J]. Current Pharmaceutical Design, 2008, 14(14): 1443 – 1451.
[47] BITTO A, GIULIANI D, PALLIO G, *et al.* Effects of COX1-2/5-LOX blockade in Alzheimer transgenic 3xTg-AD mice[J]. Inflammation Research, 2017, 66(5): 389 – 398.
[48] CHEN Q, LIANG B, WANG Z, *et al.* Influence of four polymorphisms in *ABCA*1 and *PTGS*2 genes on risk of Alzheimer's disease: a meta-analysis[J]. Neurological Sciences, 2016, 37(8): 1209 – 1220.
[49] GUAN PP, WANG P. Integrated communications between cyclooxygenase-2 and Alzheimer's disease[J]. The FASEB Journal, 2018, 33(1): 13 – 33.
[50] MA SL, TANG NL, ZHANG YP, *et al.* Association of prostaglandin-endoperoxide synthase 2 (PTGS2) polymorphisms and Alzheimer's disease in Chinese[J]. Neurobiology of Aging, 2008, 29(6): 856 – 860.
[51] ZIPFEL P, ROCHAIS C, BARANGER K, *et al.* Matrix metalloproteinases as new targets in Alzheimer's disease: Opportunities and challenges [J]. Journal of Medicinal Chemistry, 2020, 63(19): 10705 – 10725.
[52] HERNANDEZ-GUILLAMON M, MAWHIRT S, BLAIS S, *et al.* Sequential amyloid-beta degradation by the matrix metalloproteases MMP-2 and MMP-9[J]. The Journal of Biological Chemistry, 2015, 290(24): 15078 – 15091.
[53] MIZOGUCHI H, TAKUMA K, FUKUZAKI E, *et al.* Matrix metalloprotease-9 inhibition improves amyloid beta-mediated cognitive impairment and neurotoxicity in mice[J]. The Journal of Pharmacology and Experimental Therapeutics, 2009, 331(1): 14 – 22.
[54] JAKHAR R, DANGI M, KHICHI A, *et al.* Relevance of molecular docking studies in drug designing[J]. Current Bioinformatics, 2020, 15 (4): 270 – 278.